Gravitational waves as a probe of dark matter minispikes

Kazunari Eda, yousuke Itoh, Sachiko Kuroyanagi, Joseph Silk

PHYSICAL REVIEW D **91,** 044045 (2015)

Gravitational waves as a probe of dark matter minispikes

Kazunari Eda,[1,2,*] Yousuke Itoh,[2] Sachiko Kuroyanagi,[3] and Joseph Silk[4–6]

[1]*Department of Physics, Graduate School of Science, The University of Tokyo, Tokyo 113-0033, Japan*
[2]*Research Center for the Early Universe (RESCEU), Graduate School of Science, The University of Tokyo, Tokyo 113-0033, Japan*
[3]*Department of Physics, Faculty of Science, Tokyo University of Science, 1-3, Kagurazaka, Shinjuku-ku, Tokyo 162-8601, Japan*
[4]*Institut d' Astrophysique, UMR 7095, CNRS, UPMC Université. Paris VI, 98 bis Boulevard Arago, Paris 75014, France*
[5]*Department of Physics and Astronomy, The Johns Hopkins University, Baltimore, Maryland 21218, USA*
[6]*Beecroft Institute for Particle Astrophysics and Cosmology, Department of Physics, University of Oxford, Keble Road, Oxford OX1 3RH, United Kingdom*

(Received 18 August 2014; published 27 February 2015)

Recent studies show that an intermediate mass black hole (IMBH) may develop a dark matter (DM) minihalo according to some BH formation scenarios. We consider a binary system composed of an IMBH surrounded by a DM minispike and a stellar mass object orbiting around the IMBH. The binary evolves due to gravitational pull and dynamical friction from the DM minispike and backreaction from its gravitational wave (GW) radiation which can be detected by future space-borne GW experiments such as eLISA/NGO. We consider a single power-law model for the DM minispike which is assumed to consist of nonannihilating DM particles and derive GW waveforms including the DM effects analytically. We demonstrate that a detection of GWs from such a binary with eLISA/NGO is affected by the DM effects and enables us to measure the DM minispike parameters accurately. For instance, in our reference case originally advocated by Zhao and Silk [Phys. Rev. Lett. 95, 011301 (2005)] and Bertone *et al*. [Phys. Rev. D 72, 103517 (2005)], we could determine the power-law index α of the DM minispike radial profile with a 1σ relative error of $\pm 5 \times 10^{-6}$ for a GW signal with signal-to-noise ratio 10 and assuming a five-year observation with eLISA. We also investigate how accurately the DM parameters can be determined for various values of the slope of the DM minispike and the masses of the IMBH–stellar mass object binary surrounded by the DM minispike. We find that the power-law index α is measurable at 10% level even for a slightly flatter radial distribution of $\alpha \sim 1.7$. We clarify that the larger masses of the IMBH and the stellar object lead to the worse measurement accuracies of the DM parameters because the number of GW cycles becomes smaller.

DOI: 10.1103/PhysRevD.91.044045 PACS numbers: 04.30.-w, 95.35.+d, 95.85.Sz, 97.60.Lf

I. INTRODUCTION

There is much reliable evidence for the existence of dark matter (DM) which is mainly associated with the missing mass problem. Astronomers and particle physicists seek to probe DM properties by direct laboratory experiments or indirect observations [1]. Indirect techniques include efforts to detect gamma rays from DM annihilation using telescopes such as the Fermi Large Area Telescope (Fermi-LAT, [2]), the Major Atmospheric Gamma-ray Imaging Cherenkov (MAGIC) telescope [3], the High Energy Stereoscopic System (H.E.S.S., [4]) and the Very Energetic Radiation Imaging Telescope Array System (VERITAS, [5]) (see, e.g., [6] for a review).

It was first suggested by Gondolo and Silk [7] that adiabatic growth of a BH at the center of a DM halo whose density had a singular power-law cusp $\rho(r) \propto r^{-\alpha_{\rm ini}}$ with $0 \leq \alpha_{\rm ini} \leq 2$ led to a high-density DM region around the central BH, $\rho_{\rm spike}(r) \propto r^{-\alpha}$ with $2.25 \leq \alpha \leq 2.5$. This region is called a DM spike. Inside the spike, DM annihilations are enhanced and produce the strong gamma-ray photon flux which could be detectable to the telescopes mentioned above.

However, subsequent studies pointed out that this spike could be weakened by dynamical processes such as mergers of host galaxies, subhalo accretion and passing of molecular clouds [8–12]. These processes transfer energy to the DM particles and destroy the structure of the DM spike. Then the annihilation rate in the spike is smaller than predicted in [7] because it depends on the line-of-sight integral of the squared density of the spike. If supermassive black holes (SMBHs) have experienced mergers, they are unlikely to have surviving spike structure. Even this, however, is controversial because of the uncertainty in whether the final parsec problem for SMBH mergers has been resolved phenomenologically [13] or even theoretically [14]. On the other hand, formation scenarios of intermediate-mass black holes (IMBH) which

*eda@resceu.s.u-tokyo.ac.jp

allow DM minispikes have been proposed [15,16]. If the IMBH have never experienced mergers in the past, the DM minispike around the central IMBH is likely to survive.

IMBHs may exist in our Universe [17–19], and even several hundreds would reside in the halo of the present-day Milky Way galaxy [20,21]. Those IMBHs in globular clusters are recognized as promising sources for the evolved Laser Interferometer Space Antenna (eLISA) [22]/the New Gravitational Wave Observatory (NGO) [23] and DECihertz Interferometer Gravitational Wave Observatory (DECIGO)[24].

In our previous work [25], we demonstrated that a very tiny effect such as the gravitational pull of a DM minispike around an IMBH indeed affects detectability of GW by eLISA, and thereby we could infer presence or absence of a DM minispike around an IMBH using GW. Specifically, when a stellar mass object inspirals into the central IMBH, it is affected by the gravitational force of not only the central IMBH but also the minispike. Therefore, the inspiral GW is modified by the minispike around the central IMBH. We found that the very tiny effect from gravitational pull of a DM minispike could have a large impact on detectability of the GW, thanks to the huge number of orbital cycles which the binary experienced in the eLISA detection frequency band. We also found that GW detectability strongly depends on the density profile of the DM minispike.

In this paper, we extend our previous work in the following way. We again consider GWs emitted from a binary system consisting of a stellar mass object and an IMBH harbored in a DM minispike, and calculate the GW waveform including the effect of both the gravitational potential and the dynamical friction on the falling stellar mass object in the DM minispike. Furthermore, we investigate how accurately the DM parameters are determined by the GW observations. We find that the DM information contained in the waveform can be extracted with very good accuracy by GW observations if the central IMBH has a steep density minispike. We also investigate how the detection accuracy of the DM parameters changes depending on the masses of the binary components and the density profile of the DM minispike such as the power index and overall normalization.

Recently Macedo *et al*. made clear the importance of the dynamical friction on the GW waveform in a quite different context from ours, namely, a stellar mass object falling in a compact configuration of DM clouds [26]. Also, Barausse *et al.* has given a wide survey on astrophysical environmental effects on GW signals using order of magnitude estimates, concluding that astrophysical environmental effects such as accretion disks, magnetic fields, and DM halos do not obscure gravitational wave astrophysics, e.g., precision measurements of binary masses and tests of general relativity [27] (see also [28]). To indicate one exception, our paper shall clearly show that, in the recently advocated DM minispike scenario, environmental effects do affect GW detectability [25] and we can measure DM properties quite accurately from eLISA GW detection, which will be shown through a detailed study using a matched filtering technique and Fisher matrix analysis.

The rest of the paper is organized as follows. Section II presents the DM minispike model and candidates for the stellar mass object. In Sec. III we derive the GW waveform from the system which we consider, and the observational errors of the waveform parameters are calculated in Sec. IV. Finally, our conclusions are given in Sec. V.

II. MINIHALO MODEL

In this section, we provide a model of DM minihalo to evaluate the effect of the DM minihalo on GW observations. The DM halo profiles have been investigated via cosmological *N*-body simulations. Navarro, Frenk and White (NFW) have pointed out the existence of a universal density profile for DM halos and proposed the NFW profile [29]. Later work shows that the inner slope may be different from the NFW one and may not even be universal [30]. More recent simulations have suggested that alternative models such as the Einasto model could be better-fitted than the NFW one [31]. However, the DM profile in the vicinity of the central BH has yet to be investigated due to the lack of the resolution in *N*-body simulations. To handle the DM minihalo profile around the BH, we put the following two assumptions on the DM profile. The first is a single power-law model of a DM minispike. The second is that normalization factors of the DM minispike are set through the NFW profile for simplicity. Therefore, we consider various values of the slope of the minispike with the fixed normalization factors computed based on the NFW profile. The result we will present later in this paper can be easily extended to other DM profiles just by changing the normalization factors as long as the inner DM profiles can be approximately described by a single power law.

A. Initial DM minihalo profile

We assume that the initial DM minihalo profile which leads to the DM minispike after the adiabatic growth of the IMBH is approximately described by the NFW profile [29]

$$\rho_{\rm NFW}(r) = \frac{\rho_s}{(r/r_s)(1+r/r_s)^2}, \tag{1}$$

where r is the radius, ρ is the mass density and the subscript "s" stands for the scaling. The NFW parameters ρ_s and r_s are related to the cluster mass and concentration parameters by

$$M_{\rm vir} = \frac{4\pi}{3}\Delta_{\rm vir}\Omega_m(z_f)\rho_{\rm cri}(z_f)r_{\rm vir}^3, \tag{2a}$$

$$\rho_s \equiv \frac{1}{3f(c_{\rm vir})}\Delta_{\rm vir}\Omega_m(z_f)\rho_{\rm cri}(z_f)c_{\rm vir}^3, \tag{2b}$$

where $c_{\rm vir} \equiv r_{\rm vir}/r_s$ and $r_{\rm vir}$ is the virial radius and $M_{\rm vir}$ is the virial mass of the cluster, z_f is the formation redshift of the cluster, Ω_m is the matter density parameter, $\rho_{\rm cri}$ is the critical matter density of the Universe and the function $f(x)$ is the volume integral of the NFW profile $f(x) \equiv \ln(1+x) - x/(1+x)$ (see, e.g., [32]). We used the fitting formula given by [33] for the parameter $\Delta_{\rm vir}$: $\Delta_{\rm vir} \equiv 18\pi^2(1+0.4093\omega_{\rm vir}^{0.9052})$ where $\omega_{\rm vir} \equiv 1/\Omega_m(z_f) - 1$ [33]. The mass-concentration relation is taken from [34] which fits the profiles of the clusters of galaxies obtained in their N-body simulations. This result for clusters of galaxies may or may not apply for the minihalo. In any case, concentration parameters between $O(1$–$1000)$ lead to qualitatively similar results and are given by the following relation.

$$c_{200} = A_{200}(M_{200}/M_{\rm pivot})^{B_{200}}(1+z_f)^{C_{200}}, \tag{3}$$

where we assume $(A_{200}, B_{200}, C_{200}, M_{\rm pivot}) = (5.71, -0.084, -0.47, 1.0\times 10^{14}h^{-1}M_\odot)$ from the result of [34]. The parameters A_{200} and so on may be appropriately used when the overdensity $\Delta_{\rm vir}$ equals 200. However, we here assumed $A_{200} \simeq A_{\rm vir}$ and so on for simplicity.

As will be shown later, the GW waveform depends on the DM minispike slope α and some combination of the radius at which the minispike is established, $r_{\rm sp}$, and the DM density there, $\rho_{\rm sp}$. Under the assumption of adiabatic growth, while the final power-law index of the DM minispike, α, depends on the power-law index of the initial inner DM profile, the latter two depend on ρ_s, r_s and α. For concreteness, we adopt $M_{\rm vir} = M_{\rm DM} = 10^6 M_\odot$, $z_f = 20$ in Eqs. (2a), (2b), and (3) [15,16] and find $c_{\rm vir} = 6.6$, $r_s = 23.1$ pc, and $\rho_s = 3.8\times 10^{-22}$ g/cm^3.

B. DM minispike profile

We proceed to discuss the DM profile of the minispike. If the DM minihalo initially has a cuspy profile $\rho(r) \propto r^{-\alpha_{\rm ini}}$ with $0 \le \alpha_{\rm ini} \le 2$, then the adiabatic growth of the central IMBH produces the DM minispike. Hence, the dark matter profile becomes [7,35]

$$\rho_{\rm DM}(r) = \begin{cases} \rho_{\rm spike}(r), & (r_{\rm min} \le r \le r_{\rm sp}), \\ \rho_{\rm NFW}(r), & (r_{\rm sp} < r), \end{cases} \tag{4}$$

with

$$\rho_{\rm spike}(r) = \rho_{\rm sp}\left(\frac{r_{\rm sp}}{r}\right)^{\alpha}, \tag{5a}$$

$$\alpha = \frac{9-2\alpha_{\rm ini}}{4-\alpha_{\rm ini}}, \tag{5b}$$

where $\rho_{\rm sp}$ is the normalization constant and $r_{\rm sp}$ is empirically defined by $r_{\rm sp} \sim 0.2 r_h$. The radius r_h is the distance of the gravitational influence of the central IMBH with the mass $M_{\rm BH}$ and is approximately obtained by $M(<r_h) = 4\pi\int_0^{r_h}\rho_{\rm DM}(r)r^2dr = 2M_{\rm BH}$ [36]. The slope of the DM minispike takes the value $2.25 \le \alpha \le 2.5$ for $0 \le \alpha_{\rm ini} \le 2$. In the case of an initial NFW profile, $\alpha_{\rm ini} = 1$, this gives rise to $\alpha = 7/3$. If the initial profile of the minihalo is a uniform distribution, then the final profile after the adiabatic growth of the IMBH would become a more gentle $\rho_{\rm spike}(r) \propto (r/r_h)^{-3/2}$ [9,37,38].

It is important to note that the final profile of the DM minihalo depends on the formation history of the central IMBH. If the IMBH has experienced disruptive processes such as mergers in the past, the minispike would be weakened or disappear. For this reason, we do not specify the value of the power-law index α of the DM minispike and treat it as a free parameter within the range $0 \le \alpha \le 3$. In the following, even if $\alpha < 2.25$, we will still call the DM distribution close to the central IMBH described by Eq. (5a) "a DM minispike" for the sake of simplicity. Indeed we will see that the "DM minispike" leaves its signature in the GW waveform when $\alpha \gtrsim 1.7$, but certainly does not when $\alpha = 0$. We will also assume different values of $\rho_{\rm sp}$ to study how the ambiguities in ρ_s and r_s mentioned above affect our results. Finally, we take $r_{\rm min}$ to be the innermost stable circular orbit (ISCO) of the central IMBH, $r_{\rm min} = r_{\rm ISCO} \equiv 6GM_{\rm BH}/c^2$. It may be more precise to use $4GM_{\rm BH}/c^2$ [39], but such a change of $r_{\rm min}$ does not alter at all the measurement accuracy of the DM parameters shown below. The parameters of the DM density profile are summarized in Table I below.

C. Candidate for a stellar mass object

Before moving onto the calculation of the GW waveform, we discuss what can be a candidate for a stellar mass object. Let us consider a stellar mass object with mass μ denoted by A, orbiting around an intermediate mass black hole B with mass $M_{\rm BH}$. We consider the inspiral up to the innermost stable circular orbit $r_{\rm ISCO}$:

$$r_{\rm ISCO} = \frac{6GM_{\rm BH}}{c^2} \simeq 9\times 10^3\ {\rm km}\left(\frac{M_{\rm BH}}{10^3 M_\odot}\right). \tag{6}$$

TABLE I. Our reference model parameters of the IMBH, the DM minihalo and the DM minispike. $M_{\rm DM}$: The total mass of the minihalo, $M_{\rm BH}$: the mass of the central intermediate mass black hole, z_f: the formation redshift of the minihalo, $c_{\rm halo}$: the concentration of the minihalo, $r_{\rm vir}$: the virial radius of the minihalo, r_s: the NFW r_s parameter of the minihalo, ρ_s: the NFW ρ_s parameter of the minihalo, r_h: the radius at which $M_{\rm DM}(r_h) = 2M_{\rm BH}$, $r_{\rm sp}$: the radius where the spike forms (estimated by $r_{\rm sp} = 0.2r_h$), and $\rho_{\rm sp}$: the minihalo mass density at $r_{\rm sp}$.

$M_{\rm DM}$	$M_{\rm BH}$	z_f	$c_{\rm halo}$	$r_{\rm vir}$
$10^6 M_\odot$	$10^3 M_\odot$	20	6.6	152.6 pc
r_s	ρ_s	r_h	$r_{\rm sp}$	$\rho_{\rm sp}$
23.1 pc	3.8×10^{-22} g/cm^3	1.65 pc	0.54 pc	$226 M_\odot/pc^3$

Hence, the object A should have a radius smaller than at most 9×10^3 km. At the same time, the tidal radius of A orbiting B at the orbital radius of $r_{\rm ISCO}$ is

$$l_{\rm A\,tidal} \simeq r_{\rm ISCO}\left(\frac{\mu}{M_{\rm BH}}\right)^{1/3} \simeq 9\times 10^2\ {\rm km}\left(\frac{\mu}{1M_\odot}\right)^{1/3}\left(\frac{M_{\rm BH}}{10^3 M_\odot}\right)^{-1/3}\left(\frac{M_{\rm BH}}{10^3 M_\odot}\right). \tag{7}$$

Hence, this object must be either a black hole or a neutron star. Alternatively, if we assume A to be a white dwarf of radius $l_A = 10000$ km or a sunlike object of radius $l_A = 10^6$ km, the innermost orbital radius should be replaced by the radius below which the object A is tidally destroyed:

$$r_{\rm tidal} \simeq \left(\frac{M_{\rm BH}}{\mu}\right)^{1/3} l_A \simeq 3\times 10^{-7}\ {\rm pc}\left(\frac{M_{\rm BH}}{10^3 M_\odot}\right)^{1/3}\left(\frac{\mu}{1M_\odot}\right)^{-1/3}\left(\frac{l_A}{10^6\ {\rm km}}\right). \tag{8}$$

As will be stated, we will consider the orbital radius of order 10^{-8} pc or less, so we cannot assume our stellar mass object to be a normal star with radius $\sim 10^6$ km. A white dwarf may be an interesting candidate since an electromagnetic counterpart may be expected when it is tidally disrupted (e.g., [40–42]). Yet, here in this paper we assume a neutron star or a black hole when we refer to a stellar mass object.

III. GW WAVEFORM

A. Equation of motion for the stellar mass object

Let us consider a binary system which involves a small compact object with a mass of $\mu = 1M_\odot$ and an IMBH with a mass of $M_{\rm BH} = 10^3 M_\odot$. The mass of the stellar mass object μ is much smaller than the mass of IBMH $M_{\rm BH}$. So the reduced mass is approximately equal to μ and the barycenter position is approximately equal to the position of the IMBH. By adopting a reference frame attached to the barycenter, the equation of motion of the radial relative separation between the stellar mass object and the IMBH describes the motion of the former and is given by

$$\frac{d^2 r}{dt^2} = -\frac{GM_{\rm eff}}{r^2} - \frac{F}{r^{\alpha-1}} + \frac{h^2}{r^3}, \tag{9}$$

where h is the angular momentum of the stellar mass object per its mass, and $M_{\rm eff}$ and F are defined by

$$M_{\rm eff} = \begin{cases} M_{\rm BH} - M_{\rm DM}(<r_{\rm min}) & (r_{\rm min} \le r \le r_{\rm sp}), \\ M_{\rm BH} & (r < r_{\rm min}), \end{cases} \tag{10a}$$

$$F = \begin{cases} r_{\rm min}^{\alpha-3} M_{\rm DM}(<r_{\rm min}) & (r_{\rm min} \le r \le r_{\rm sp}), \\ 0 & (r < r_{\rm min}). \end{cases} \tag{10b}$$

The mass $M_{\rm DM}(< r_{\rm min})$ denotes the DM mass contained within the ISCO and is defined as $M_{\rm DM}(<r_{\rm min}) \equiv 4\pi r_{\rm sp}^\alpha \rho_{\rm sp} r_{\rm min}^{3-\alpha}/(3-\alpha)$. The first term on the right-hand side of Eq. (9) describes the gravitational potential of the effective mass of the central IMBH which is modified by the DM due to the absence of the DM within the ISCO, the second term accounts for the DM effect, and the third term represents a centrifugal force. Here the dynamical friction force and the GW backreaction force are neglected because these effects are much smaller than the gravitational potential of the IMBH. We will introduce these effects to include an adiabatic evolution of the orbital radius in the next subsection.

We assume that the stellar mass object orbits in a circular manner for simplicity. The orbital radius R is obtained by solving $d^2 r/dt^2 = 0$ in Eq. (9). The orbital frequency ω_s is related to the angular momentum h by $R\omega_s$, so we get

$$\omega_s = \left(\frac{GM_{\rm eff}}{R^3} + \frac{F}{R^\alpha}\right)^{1/2}. \tag{11}$$

When a DM minispike is not present around the IMBH, $F \to 0$ and $M_{\rm eff} \to M_{\rm BH}$, so Eq. (11) leads to the Kepler's law $\omega_s^2 = GM_{\rm BH}/R^3$.

B. Energy balance equation

In this subsection, we introduce the GW backreaction and the dynamical friction into the stellar mass object's orbit by taking the energy balance equation into account. When the stellar mass object orbits around the IMBH, a part of its energy $E_{\rm orbit}$ is converted into GW emission loss $E_{\rm GW}$ and dynamical friction loss $E_{\rm DF}$. Thus, the following energy balance equation is satisfied:

$$-\frac{dE_{\rm orbit}}{dt} = \frac{dE_{\rm GW}}{dt} + \frac{dE_{\rm DF}}{dt}. \tag{12}$$

As we will see in this subsection, this energy balance equation gives the time evolution of the orbital radius. The resulting orbit can be regarded as a quasicircular orbit because of the smallness of these dissipative effects.

The orbital energy $E_{\rm orbit}$ is the sum of the kinetic energy and the gravitational potential of the stellar mass object, so we can calculate $E_{\rm orbit}$ using Eq. (11),

$$E_{\rm orbit} = \frac{1}{2}\mu v^2 - \frac{G\mu M_{\rm eff}}{R} + \frac{1}{2-\alpha}\frac{\mu F}{R^{\alpha-2}} = -\frac{G\mu M_{\rm eff}}{2R} + \frac{4-\alpha}{2(2-\alpha)}\frac{\mu F}{R^{\alpha-2}}, \quad (13)$$

where v is the orbital velocity. When we consider the evolution of the radius R, dR/dt does not vanish. So the time derivative of Eq. (13) gives the following equation:

$$\frac{dE_{\rm orbit}}{dt} = \left(\frac{GM_{\rm eff}}{2R^2} + \frac{4-\alpha}{2}\frac{F}{R^{\alpha-1}}\right)\mu\frac{dR}{dt}. \quad (14)$$

To the lowest order in the post-Newtonian expansion, the gravitational radiation energy is given by the quadrupole formula. We apply the formula to the circular Newtonian binary and obtain

$$\frac{dE_{\rm GW}}{dt} = \frac{32}{5}\frac{G\mu^2}{c^5}R^4\omega_s^6. \quad (15)$$

When the stellar mass object moves through the cloud of DM, it gravitationally interacts with DM particles. This effect is called dynamical friction, sometimes referred to as gravitational drag which was first discussed by Chandrasekhar [43]. Because of dynamical friction, the stellar mass object running through the DM halo is decelerated in the direction of its motion and loses its kinetic energy as well as its angular momentum. The dynamical friction force is given by $f_{\rm DF} = 4\pi G^2\mu^2\rho_{\rm DM}(r)\ln\Lambda/v^2$ where v is the velocity of the stellar mass object [44]. The Coulomb logarithm Λ is defined by $\lambda \cong b_{\rm max}v_{\rm typ}^2/(G\mu)$ where $b_{\rm max}$ is the maximum impact parameter and $v_{\rm typ}$ is the typical velocity of the stellar mass object. We take $\ln\Lambda \cong 3$. From the expression of the dynamical friction force, we obtain the friction loss,

$$\frac{dE_{\rm DF}}{dt} = vf_{\rm DF} = 4\pi G^2\frac{\mu^2\rho_{\rm DM}(r)}{v}\ln\Lambda. \quad (16)$$

To find the numerical solution of the energy balance equation (12) easily, we introduce a dimensionless radius parameter x defined by

$$x \equiv \varepsilon^{1/(3-\alpha)}R, \quad (17)$$

with

$$\varepsilon \equiv \frac{F}{GM_{\rm eff}}. \quad (18)$$

Using the above definition of x, the energy balance equation (12) can be rewritten in the form of the differential equation of x with respect to time t as

$$\frac{dx}{dt} = -c_{\rm GW}\frac{(1+x^{3-\alpha})^3}{4x^3[1+(4-\alpha)x^{3-\alpha}]} - c_{\rm DF}\frac{1}{(1+x^{3-\alpha})^{1/2}[1+(4-\alpha)x^{3-\alpha}]x^{-5/2+\alpha}}, \quad (19)$$

where the coefficients are defined by

$$c_{\rm GW} \equiv \frac{256}{5}\left(\frac{G\mu}{c^3}\right)\left(\frac{GM_{\rm eff}}{c}\right)^2\varepsilon^{4/(3-\alpha)}, \quad (20a)$$

$$c_{\rm DF} \equiv (8\pi G^2\mu\rho_{\rm sp}r_{\rm sp}^{\alpha}\ln\Lambda)(GM_{\rm eff})^{-3/2}\varepsilon^{(2\alpha-3)/[2(3-\alpha)]}. \quad (20b)$$

The coefficient $c_{\rm GW}$ is related to the gravitational radiation energy and the coefficient $c_{\rm DF}$ is related to the dynamical friction. In the case of the initial NFW profile, $\alpha = 7/3$, the coefficients $c_{\rm GW}$ and $c_{\rm DF}$ are $c_{\rm GW} = 2.0\times10^{-33}[1/{\rm year}]$, $c_{\rm DF} = 2.1\times10^{-8}[1/{\rm year}]$. Note that the dynamical friction coefficient $c_{\rm DF}$ is much larger than the gravitational radiation coefficient $c_{\rm GW}$.

C. GW waveform

The GW waveform from the binary composed of two compact objects with masses μ and $M_{\rm BH}$ is given by

$$h_+(t) = \frac{1}{D}\frac{4G\mu\omega_s^2R^2}{c^4}\frac{1+\cos^2\iota}{2}\cos(\omega_{\rm GW}t), \quad (21a)$$

$$h_\times(t) = \frac{1}{D}\frac{4G\mu\omega_s^2R^2}{c^4}\cos\iota\sin(\omega_{\rm GW}t), \quad (21b)$$

where D is the distance to the source (luminosity distance for a cosmological source), R is the orbital radius, ι is the inclination angle, which is the angle between the line-of-sight and the rotational axis of the orbits, and $\omega_{\rm GW}$ is the GW frequency which is given by $\omega_{\rm GW} \equiv 2\omega_s$ [45].

The waveforms Eqs. (21a) and (21b) are derived on the assumption that the motion of the source is described by a circular Newtonian orbit. But in fact, the radius R and the frequency ω_s are not constant because the orbital energy $E_{\rm orbit}$ decreases gradually due to both the dynamical friction and the GW backreaction. Including these effects, the orbit shrinks adiabatically and becomes a quasicircular orbit. So the radius R and the frequency ω_s should be replaced by $R \to R(t)$, $\omega_s \to \omega_s(t)$, and the phase $\omega_{\rm GW}t$ should also be replaced by $\omega_{\rm GW}t \to \Phi(t)$ as defined by Eq. (22c) below. Thus, the GW waveform is expressed by

$$h_+(t) = \frac{1}{D}\frac{4G\mu\omega_s(t)^2R(t)^2}{c^4}\frac{1+\cos^2\iota}{2}\cos[\Phi(t)], \quad (22a)$$

$$h_\times(t) = \frac{1}{D}\frac{4G\mu\omega_s(t)^2R(t)^2}{c^4}\cos\iota\sin[\Phi(t)], \quad (22b)$$

$$\Phi(t) \equiv \int^t \omega_{\rm GW}(t')dt'. \quad (22c)$$

In order to discuss detectability and parameter accuracy in GW observations, it is convenient to work in the frequency domain. The Fourier transformation of the GW waveform is given by

$$\tilde{h}_{+,\times}(f) = \int_{-\infty}^{\infty} h_{+,\times}(t) e^{2\pi i f t} dt, \tag{23}$$

where f is the GW frequency. For simplicity, we consider a GW coming in the detector from the optimal direction for + mode. In such a situation, detector pattern functions are $F_+ = 1$ and $F_\times = 0$. So the response of the detector to the GW is $h(t) = h_+(t)$. Using Eq. (22a), we rewrite the GW waveform as

$$h(t) = A(t_{\rm ret}) \cos \Phi(t_{\rm ret}), \tag{24a}$$

$$A(t) \equiv \frac{1}{D} \frac{4G\mu\omega_s^2(t) R^2(t)}{c^4} \frac{1+\cos^2\iota}{2}, \tag{24b}$$

where $A(t)$ is the time-dependent amplitude, and $\Phi(t)$ is the time-dependent GW phase. In the above equations, we have introduced the retarded time $t_{\rm ret} \equiv t - D/c$. At the frequency of interest, the time-dependent amplitude $A(t)$ varies slowly, while the time-dependent phase $\Phi(t)$ varies rapidly. So, the Fourier transformation of the GW waveform can be calculated approximately using the stationary phase method. In this method, the rapidly oscillating term is neglected and only the slowly oscillating term survives. Then the GW waveform in the Fourier domain becomes

$$\tilde{h}(f) = \frac{1}{2} e^{i\Psi(t)} A(t) \left[\frac{2\pi}{\ddot{\Phi}(t)}\right]^{1/2}, \tag{25a}$$

$$\Psi(t) = 2\pi f \frac{D}{c} + \tilde{\Phi}(t) - \frac{\pi}{4}, \tag{25b}$$

$$\tilde{\Phi}(t) \equiv 2\pi f t - \Phi(t), \tag{25c}$$

where the time t is related to frequency by $2\pi f = \omega_{\rm gw}(t)$ [46].

As we will discuss in Appendix A, the GW waveform Eqs. (25a), (25b) and (25c) can be rewritten explicitly in the frequency domain as follows:

$$\tilde{h}(f) = \mathcal{A} f^{-7/6} e^{i\Psi(f)} \chi^{19/4} [K(x)(1+\tilde{c}J(x))]^{-1/2}, \tag{26a}$$

$$\mathcal{A} = \left(\frac{5}{24}\right)^{1/2} \frac{1}{\pi^{2/3}} \frac{c}{D} \left(\frac{GM_c}{c^3}\right)^{5/6} \frac{1+\cos^2\iota}{2}, \tag{26b}$$

$$\Psi(f) = 2\pi f \tilde{t}_c - \Phi_c - \frac{\pi}{4} - \tilde{\Phi}(f), \tag{26c}$$

$$\tilde{\Phi}(f) = \frac{10}{3} \left(\frac{8\pi G M_c}{c^3}\right)^{-5/3} \left[-f \int_\infty^f df' \frac{\chi^{11/2}}{f'^{11/3} K(1+\tilde{c}J)} + \int_\infty^f df' \frac{\chi^{11/2}}{f'^{8/3} K(1+\tilde{c}J)}\right], \tag{26d}$$

$$J(x) = \frac{4x^{11/2-\alpha}}{(1+x^{3-\alpha})^{7/2}}, \tag{26e}$$

$$K(x) = \frac{(1+x^{3-\alpha})^{5/2}(1+\alpha x^{3-\alpha}/3)}{1+(4-\alpha)x^{3-\alpha}}, \tag{26f}$$

$$\chi = (\delta\varepsilon)^{1/(\alpha-3)} x, \tag{26g}$$

$$\delta = \left(\frac{GM_{\rm eff}}{\pi^2 f^2}\right)^{(3-\alpha)/3}, \tag{26h}$$

where $\mathcal{A}$ is the overall amplitude, M_c is the chirp mass defined by $M_c \equiv \mu^{3/5} M_{\rm eff}^{2/5}$, $\tilde{t}_c$ is the sum of the binary coalescence time t_c and D/c, Φ_c is the phase at coalescence, α is the power-law index of the DM minispike, $\tilde{c}$ is defined by $\tilde{c} \equiv c_{\rm DF}/c_{\rm GW}$, δ is a new frequency variable, x is defined in Eq. (17), and ε is defined by Eq. (18). The DM information is encoded in the waveform Eq. (26a) through $K(x)$, $J(x)$, χ, $\tilde{c}$ and $M_{\rm eff}$. So if we take $K(x) \to 1$, $\chi \to 1$, $\tilde{c} \to 0$, $M_{\rm eff} \to M_{\rm BH}$, then Eq. (26a) becomes the waveform without the DM shown in Eqs. (A15a)–(A15d).

D. $\delta\varepsilon$ expansion

As we will discuss in the next section, we consider a five-year observation by eLISA which corresponds to $f \gtrsim 10^{-3}$ Hz. In this setup, $\delta\varepsilon \ll 1$ is satisfied. For example, we get $\delta\varepsilon = 3.5 \times 10^{-6}$ for $\alpha = 7/3$, $f = 0.01$ Hz, $\mu = 1M_\odot$ and the parameters $\rho_{\rm sp}$, $r_{\rm sp}$, and $M_{\rm BH}$ listed in Table I. So the product $\delta\varepsilon$ can be treated as a small dimensionless expansion parameter. Note that ε is of the order of 1 but δ is much smaller than 1 at the frequency of interest. The product $\delta\varepsilon$ represents deviations from the case without the DM minispike. Since the measurement errors of the physical parameters contained in the GW are much more sensitive to the GW phase rather than its amplitude, we expand the GW waveform $\tilde{h}(f)$ up to the first order in $\delta\varepsilon$ in the phase and up to the zeroth order in the amplitude. Using an expansion of χ in $\delta\epsilon$,

$$\chi = 1 + \frac{1}{3}\delta\varepsilon + \frac{2-\alpha}{9}\delta^2\varepsilon^2 + \cdots, \tag{27}$$

the GW waveform given by Eqs. (26a)–(26h) becomes

$$\tilde{h}(f) = \mathcal{A} f^{-7/6} e^{i\Psi(f)}, \tag{28a}$$

$$\tilde{\Phi}(f) = \frac{10}{3} \left(\frac{8\pi G M_c}{c^3}\right)^{-5/3} \left[-f \int_{f_{\rm ISCO}}^f df' f'^{-11/3} L^{-1}(f') + \int_{f_{\rm ISCO}}^f df' f'^{-8/3} L^{-1}(f')\right], \tag{28b}$$

$$L(f) = 1 + 4c_\varepsilon \tilde{\delta}^{(11-2\alpha)/[2(3-\alpha)]}, \tag{28c}$$

$$\tilde{\delta} = \left(\frac{G}{\pi^2 f^2}\right)^{(3-\alpha)/3}, \tag{28d}$$

$$c_\varepsilon = M_{\rm eff}^{(11-2\alpha)/6}\tilde{c}\varepsilon^{(11-2\alpha)/[2(3-\alpha)]} = 5\pi c^5 G^{-5/2} M_{\rm eff}^{-(\alpha+5)/3}\rho_{\rm sp} r_{\rm sp}^{\alpha} \ln\Lambda, \tag{28e}$$

where the overall amplitude $\mathcal{A}$ is defined by Eq. (26b) and $\Psi(f)$ is defined by Eq. (26c). The upper bound of the integration in Eq. (28b), $f_{\rm ISCO} > f$ in the eLISA frequency band, is the GW frequency when the stellar mass object enters the innermost stable circular orbit. Hence, $\tilde{\Phi}(f)/(2\pi)$ is in essence the GW cycles from the frequency f to the coalescence. In the above equations, the post-Newtonian (PN) effects which are neglected must be taken into account in real data analysis. However, the frequency dependence of the PN effect in the GW phase $\tilde{\Phi}(f)$ differs from that of the DM effect which depends on the power-law index α. So, the measurement accuracies of the DM parameters as we will discuss later would not be affected seriously by higher-order terms in the PN expansion.

Until the previous sections, we have included both the dynamical friction and the gravitational pull of the DM minispike. It is easily shown that the dynamical effect has much more impact on the measurement accuracy of the DM parameters than the DM minispike does [28], and the above expression indeed includes the dynamical friction but not the gravitational pull of the DM minispike. Within the approximation in this subsection and the following, the gravitational potential of the DM minispike shows its signature mainly in the IMBH mass redefinition ($M_{\rm BH} \to M_{\rm eff}$ in M_c in the above equations). We, however, note that even such a tiny effect as the gravitational pull of the DM minispike does affect the detectability of GW thanks to the large number of the GW cycles in the eLISA detection band [25].

It should be noted that all the effects of the DM are characterized by the function $L(f)$ and that it consists of two DM parameters, α and c_ε. We make use of the above equations to calculate measurement errors of the waveform parameters in the next section. We also define the phase difference $\Delta\tilde{\Phi}(f)$ by

$$\Delta\tilde{\Phi}(f) \equiv \tilde{\Phi}(f) - \tilde{\Phi}_0(f), \tag{29}$$

where $\tilde{\Phi}(f)$ defined by Eq. (28b) is the phase including the DM effect, and $\tilde{\Phi}_0(f)$ defined by Eq. (A15d) is the phase without the DM effect. $\Delta\tilde{\Phi}(f)$ is shown in Fig. 1 which indicates that the phase difference becomes significant for large α and for the large GW frequency f. This is because in this case, the DM density near the central BH increases and the effect of the DM on the motion of the stellar mass object is significant. Figure. 1 can be directly compared with Fig. 1 in our previous paper [25]. For example, in the case of [25] in which the dynamical friction is not taken into account, the phase difference $\Delta\Psi$ is of the order of 0.1 at 0.1 Hz for $\alpha = 7/3$, while in the present of the dynamical friction, shown here in Fig. 1, $\Delta\Psi$ is of the order of 10^4. This comparison implies that the effect of the dynamical friction overwhelms that of the gravitational pull. As discussed in [25], the phase difference causes the mismatch between the waveform including the DM effect and the waveform without the DM effect. The phase difference $\Delta\tilde{\Phi}(f)$ typically above 1 indicates the necessity to use the waveform including the DM effect as a template. As can be seen in Fig. 1, if the template without the DM effect is applied to the GW signal affected by the DM with $\alpha > 1.5$, the resulting signal-to-noise ratio (S/N) would be degraded significantly due to the phase difference $\Delta\tilde{\Phi}(f)$.

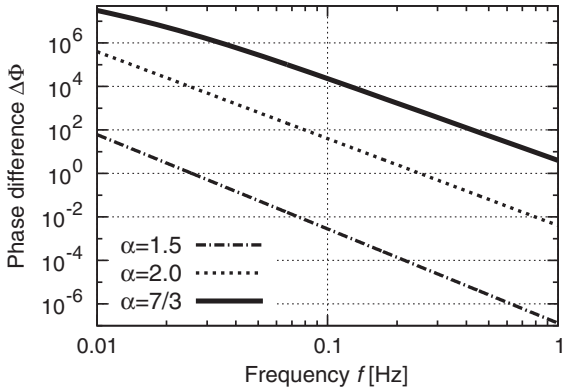

FIG. 1. The accumulated phase difference $\Delta\tilde{\Phi}$ against the power-law index α, defined by Eq. (29). In essence, this is the difference between the accumulated phase from GW frequency f and the binary coalescence with and without the DM minispike. Three different curves show $\Delta\tilde{\Phi}$ for three different values of α. For instance, if detecting a binary GW from $f = 0.01$ Hz to its coalescence, we would observe by a factor of 10^7 more GW cycles in the case with a $\alpha = 7/3$ DM minispike than without any. For this plot, we take $\mu = 1M_\odot$ and $\rho_{\rm sp}$, $r_{\rm sp}$, and $M_{\rm BH}$ are as listed in Table I.

IV. PARAMETER RESOLUTION FOR ELISA

A. Brief review of the Fisher analysis

In this subsection, we give a brief review of parameter estimation (see [46,47] for more details). Let us consider detecting GWs with a single detector. The detector output $s(t)$ can be written by the sum of the GW signal $h(t)$ and detector noise $n(t)$:

$$s(t) = h(t) + n(t). \tag{30}$$

Assuming that the detector noise is stationary, the correlation between different Fourier components of the noise is expressed as

$$\langle \tilde{n}(f)\tilde{n}^*(f')\rangle = \frac{1}{2}\delta(f-f')S_n(f), \tag{31}$$

where the angled brackets $\langle\rangle$ denote an ensemble average, the asterisk is complex conjugation and $S_n(f)$ is a one-sided power spectral density of the detector noise. In this paper, we consider the GW observation using eLISA which has the best sensitivity at around $f = 0.01$ [Hz]. The noise spectral density of eLISA is given by

$$S_n(f) = \frac{20}{3}\frac{4S_{\rm acc}(f)/(2\pi f)^4 + S_{\rm sn}(f) + S_{\rm omn}(f)}{\ell^2} \times \left[1 + \left(\frac{f}{0.41c/2\ell}\right)\right]^2, \tag{32a}$$

where $S_{\rm acc}(f) = 2.13\times 10^{-29}(1+10^{-4}/f)$ [m^2/s^{4}Hz] is the acceleration noise spectral density, $S_{\rm sn}(f) = 6.28\times 10^{-23}$ [m^2/Hz] is the shot noise spectral density, $S_{\rm omn}(f) = 5.25\times 10^{-23}$ [m^2/Hz] is the other measurement noise spectral density and $\ell = 10^9$ [m] is the separation between the spacecraft which is the length of its arms of the laser interferometer (see [23,48] for details).

It is convenient to introduce a noise-weighted inner product between two signals $h_1(t)$ and $h_2(t)$ by

$$(h_1|h_2) \equiv 4{\rm Re}\int_{f_{\rm ini}}^{f_{\rm ISCO}} \frac{\tilde{h}_1(f)\tilde{h}_2^*(f)}{S_n(f)}df, \tag{33}$$

where Re denotes the real part and $f_{\rm ini}$ is the initial frequency. Assuming that the detector noise is Gaussian and stationary, the probability density of the detector noise is described by $p(n) \propto e^{-(n|n)/2}$. We can rewrite this expression in the form of detector signal $s(t)$ and GWs signal $h(t)$ using Eq. (30) as $p(n) \propto e^{-(s-h|s-h)/2}$.

In the above case, $h(t)$ is known, while in actual GW experiments, $h(t)$ should be replaced with a template $h(t;\theta)$, where $\theta = \{\theta_1, \cdots, \theta_N\}$ is a collection of unknown parameters. To determine the waveform parameters θ, it is necessary to search for the parameters which minimize the logarithm of the maximum likelihood ratio, $(s-h|s-h) - (s|s)$. As a result of this process, we can infer the values of θ. However, the expected values have statistical errors because the detector noise is a random process. These measurement errors $\Delta\theta^i$ of the waveform parameters are approximately described by the Gaussian probability distribution for large S/N,

$$p(\Delta\theta^i) = \mathcal{N}\exp\left(-\frac{1}{2}\Gamma_{ij}\Delta\theta^i\Delta\theta^j\right), \tag{34}$$

where $\mathcal{N}$ is the normalization factor and Γ_{ij} is called the Fisher information matrix defined by

$$\Gamma_{ij} \equiv \left(\frac{\partial h}{\partial\theta^i}\middle|\frac{\partial h}{\partial\theta^j}\right). \tag{35}$$

The inverse of the Fisher matrix gives the root-mean-square (rms) errors of the waveform parameters θ^i,

$$\Delta\theta^i \equiv \sqrt{\langle(\Delta\theta^i)^2\rangle} = \sqrt{(\Gamma^{-1})_{ii}}, \tag{36}$$

where $(\Gamma^{-1})_{ii}$ denotes the diagonal elements of the inverse Fisher matrix.

B. Preparation for parameter estimation

The inspiral GW waveform from the IMBH surrounded by the DM minispike is described by six parameters which appear in Eqs. (28a)–(28e): the overall amplitude, $\mathcal{A}$; the time constant, $\tilde{t}_c \equiv t_c + D/c$, which is the sum of the traveling time D/c and the coalescence time t_c; the coalescence phase, Φ_c; the chirp mass, M_c; and the two DM parameters, α and c_ε. Note that the beam pattern function of eLISA is neglected here because we are concerned with how the DM parameters are determined by GW observations but not with the angular resolution of eLISA (see [49] for discussion of angular resolution).

The inner product between the derivatives of the waveform with respect to the parameters θ yields the values of the Fisher matrix elements. The derivatives with respect to $\mathcal{A}$, $\tilde{t}_c$, Φ_c and $\ln M_c$ are calculated straightforwardly as follows:

$$\frac{\partial\tilde{h}}{\partial\ln\mathcal{A}} = \tilde{h}, \tag{37a}$$

$$\frac{\partial\tilde{h}}{\partial\tilde{t}_c} = 2\pi i f\tilde{h}, \tag{37b}$$

$$\frac{\partial\tilde{h}}{\partial\Phi_c} = -i\tilde{h}, \tag{37c}$$

$$\frac{\partial\tilde{h}}{\partial\ln M_c} = \frac{5}{3}i\tilde{h}\,\tilde{\Phi}\,. \tag{37d}$$

The derivatives with respect to the DM parameters α, c_ε are obtained by applying the chain rule to the following equations:

$$\frac{\partial\tilde{h}}{\partial\ln\alpha} = \alpha\tilde{h}\left(i\frac{\partial\Psi}{\partial\alpha} - \frac{1}{2}\frac{1}{L}\frac{\partial L}{\partial\alpha}\right), \tag{38a}$$

$$\frac{\partial\tilde{h}}{\partial\ln c_\varepsilon} = c_\varepsilon\tilde{h}\left(i\frac{\partial\Psi}{\partial c_\varepsilon} - \frac{1}{2}\frac{1}{L}\frac{\partial L}{\partial c_\varepsilon}\right), \tag{38b}$$

where L is defined in Eq. (28c). However, since the explicit expressions are complicated, we take the derivatives numerically.

Next, we derive the initial frequency at which the GW observation starts. In the presence of the DM minispike, the

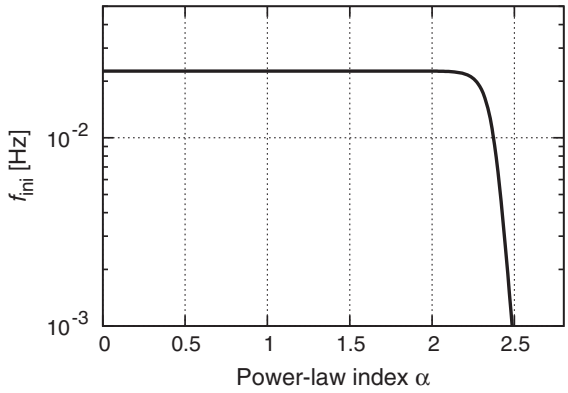

FIG. 2. Initial frequency against the power-law index α. We assume that the GW is detected by an eLISA five-year observation. For small α, $f_{\rm ini}$ is almost constant. On the other hand, for large α, $f_{\rm ini}$ drops sharply due mainly to the dynamical friction. For this plot, we take $\mu = 1M_\odot$ and $\rho_{\rm sp}$, $r_{\rm sp}$, and $M_{\rm BH}$ are as listed in Table I.

stellar mass object orbiting the central IMBH loses its angular momentum gradually due to both the dynamical friction and GW radiation reaction. So the coalescence arises earlier than the case without the DM. Time evolution of the frequency is described by Eq. (A12),

$$\frac{df}{d\tau} = -\frac{3}{5}\pi\left(\frac{f}{f_0}\right)^{5/3} f^2\chi^{-11/2}[K(1+\tilde{c}J)], \tag{39}$$

where $f_0 \equiv c^3/8\pi G M_c$ and τ is the time to the coalescence. (Note that $d\tau = -dt$.) The lower bound $f_{\rm ini}(\alpha)$ of the integral in Eq. (33) is required for calculating the inner product in the Fisher matrix. Given that the GW is observed by eLISA for five years prior to the coalescence, this bound is obtained by

$$f_{\rm ini}(\alpha) \equiv f(\alpha, \tau = 5\ [\rm yr]). \tag{40}$$

By numerically solving Eq. (39), we show the dependence of α on $f_{\rm ini}$ in Fig. 2. This figure indicates that the DM minispike affects more strongly the motion of the stellar mass object for larger α. The initial frequency for a five-year observation is almost constant for small α due to the smallness of the effect of the DM. Conversely, the initial frequency drops sharply for large α due to the dynamical friction from the DM.

C. Measurement accuracy: The case for initial NFW profile

In this subsection, we take an example of an initial NFW profile to demonstrate measurement accuracies of the waveform parameters. In this case, the slope of the DM minispike $\alpha = 7/3$. Derivatives of the waveform with respect to the parameters given by Eqs. (37a)–(38b) are calculated numerically. Substitution of these results into Eqs. (35) and (36) gives rise to the rms errors $\Delta \ln \mathcal{A}$, $\Delta\tilde{t}_c$, $\Delta\Phi_c$, $\Delta \ln M_c$, $\Delta \ln \alpha$ and $\Delta \ln c_\varepsilon$ as follows:

$$\frac{\Delta\mathcal{A}}{\mathcal{A}} = 0.1\left(\frac{10}{S/N}\right), \tag{41a}$$

$$\Delta\tilde{t}_c = 1.0[\rm s]\left(\frac{10}{S/N}\right), \tag{41b}$$

$$\Delta\Phi_c = 1.3[\rm rad]\left(\frac{10}{S/N}\right), \tag{41c}$$

$$\frac{\Delta M_c}{M_c} = 3.1\times10^{-7}\left(\frac{10}{S/N}\right), \tag{41d}$$

$$\frac{\Delta\alpha}{\alpha} = 1.2\times10^{-6}\left(\frac{10}{S/N}\right), \tag{41e}$$

$$\frac{\Delta c_\varepsilon}{c_\varepsilon} = 5.9\times10^{-5}\left(\frac{10}{S/N}\right). \tag{41f}$$

Here we take $\rho_{\rm sp}$, $r_{\rm sp}$, and $M_{\rm BH}$ from Table I and $\mu = 1M_\odot$. These measurement errors are inversely proportional to S/N. So the waveform parameters are measurable with a better accuracy for larger GW signals. A notable feature of the above results is that the chirp mass M_c and the two DM parameters α and c_ε are determined much more accurately than the overall amplitude $\mathcal{A}$, the coalescence time $\tilde{t}_c$ and the coalescence phase Φ_c. This fact reflects that M_c, α and c_ε appear in the phase of the waveform $\tilde{\Phi}(f)$. From Eqs. (B1), (22c) and (25c), the GW phase is proportional to the number of GW cycles which amplify the sensitivity to the parameters which appear in the phase $\tilde{\Phi}(f)$ by a factor $N_{\rm cycles}$. Thus, the fractional error of the chirp mass which is proportional to the phase is order of $1/N_{\rm cycle}$ and the two DM parameters are also determined very accurately. In fact, Fig. 8 indicates the value of $1/N_{\rm cycle}$ is about 10^{-7}, which is consistent with the value of $\Delta M_c/M_c$ in Eq. (41d).

We also investigate the correlation between the parameters which appear in the phase, M_c, α and c_ε. Figure 3 illustrates the Fisher ellipses for M_c, α and c_ε in $S/N = 10$. From the figures, we observe that M_c, α and c_ε are strongly correlated with each other because all of them are contained in the phase. However, they are not completely degenerate and are determined independently. This fact can be traced to the difference of the frequency dependence between M_c, α and c_ε.

In the above discussion, the mass of the central IMBH $M_{\rm BH}$ and that of the stellar mass object μ are fixed. Next we analyze the measurement errors for various values of μ and $M_{\rm BH}$. The results are shown in Fig. 4. The figure indicates the errors of the parameters in the phase $\tilde{\Phi}(f)$ increase linearly with the stellar mass object mass μ. This behavior comes

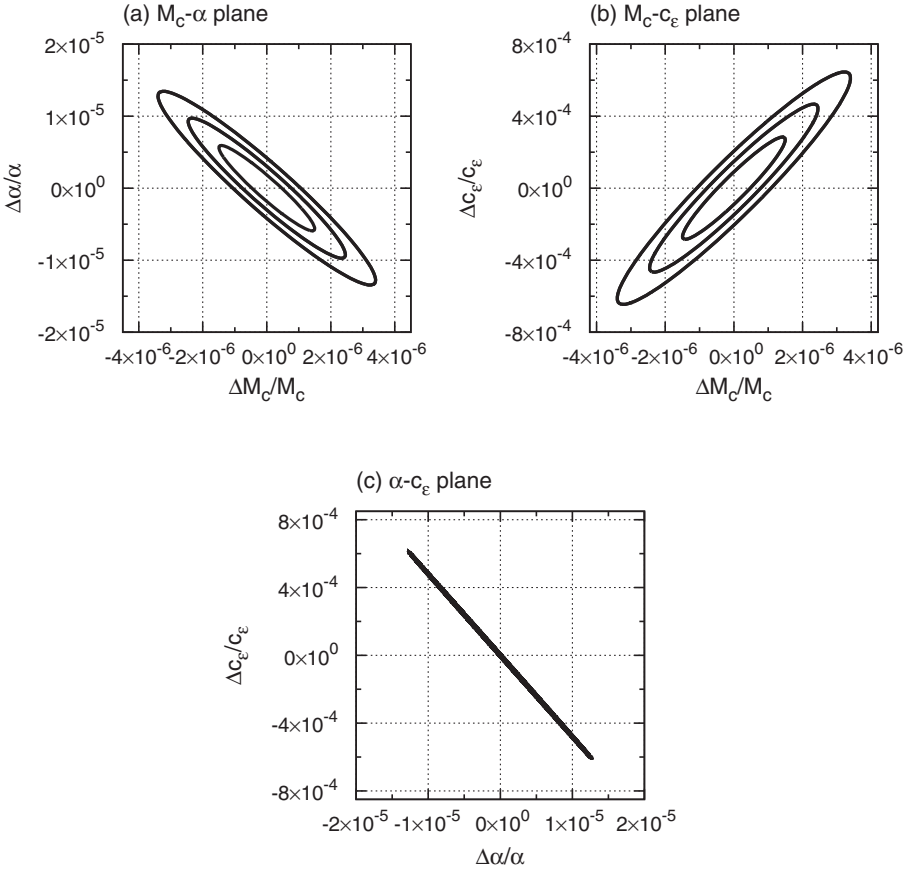

FIG. 3. Confidence level contours of 68.3%, 95.4% and 99.7% for $S/N = 10$ in the case where the initial DM halo has an NFW profile and the final profile has the radial power-law index of $\alpha = 7/3$ through an adiabatic growth. We assume $\rho_{\rm sp}$, $r_{\rm sp}$, and $M_{\rm BH}$ from Table I and $\mu = 1M_\odot$.

from the fact that the number of cycles $N_{\rm cycle}$ decreases in proportion to the stellar mass object mass μ. Similarly, the larger the mass of the IMBH, the smaller the number of the orbital cycles the stellar mass object experienced in the five years prior to the coalescence within the eLISA band. For this reason, the measurement errors in M_c, α, and c_ϵ increase for a larger IMBH mass as can be seen in Fig. 4.

D. Measurement accuracy: General case for initial DM profile

We now extend the analysis in the previous section where we considered the case of the initial NFW profile. We next consider the general case without specifying the value of α with $M_{\rm BH}$, $\rho_{\rm sp}$, and $r_{\rm sp}$ fixed to the values quoted in Table I. The rms errors depend on the DM power-law index α. We show $\Delta \ln M_c$, $\Delta \ln \alpha$ and $\ln \Delta c_\varepsilon$ in Fig. 5.

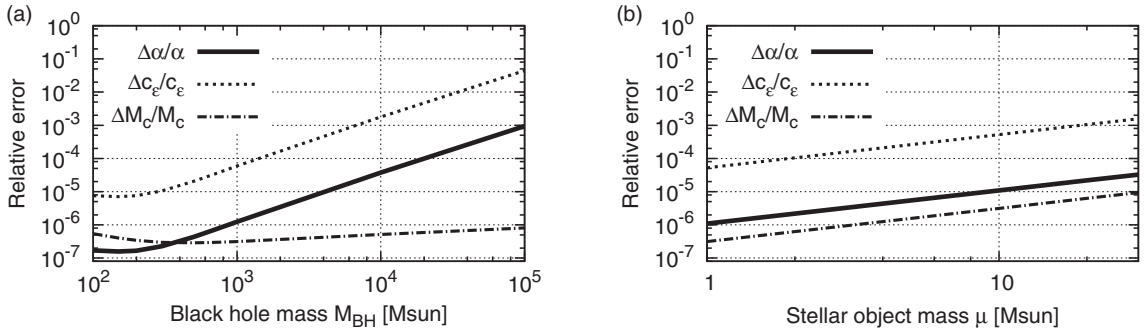

FIG. 4. The relative errors of the parameters in the phase $\tilde{\Phi}(f)$ versus (a) the central BH mass $M_{\rm BH}$ and (b) the stellar mass object mass μ for $S/N = 10$ and $\alpha = 7/3$. For this plot, $\rho_{\rm sp}$ and $r_{\rm sp}$ are taken from Table I. The other parameter is fixed to be $\mu = 1M_\odot$ in the left and $M_{\rm BH} = 10^3 M_\odot$ in the right, respectively. Note that both axes are in the logarithmic scales. The solid line, the dashed line and the dashed-dotted line correspond to $\Delta\alpha/\alpha$, $\Delta c_\varepsilon/c_\varepsilon$, $\Delta M_c/M_c$ respectively.

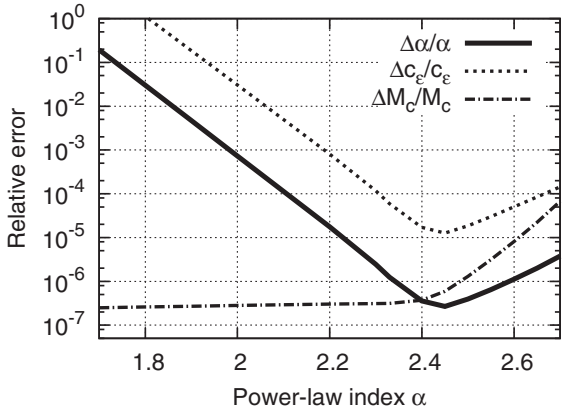

FIG. 5. The relative errors of the parameters in the phase $\tilde{\Phi}(f)$ versus the power-law index of the DM profile for $S/N = 10$ in the case where the DM minispike harboring the IMBH has a radial power-law profile. The solid line, the dashed line, and the dashed-dotted line corresponds to $\Delta\alpha/\alpha$, $\Delta c_\varepsilon/c_\varepsilon$, $\Delta M_c/M_c$ respectively. For this plot, $\mu = 1M_\odot$ and the values of the parameters $M_{\rm BH}$, $\rho_{\rm sp}$, and $r_{\rm sp}$ are assumed as in Table I.

As shown in Fig. 5, the accuracy of the DM parameters $\Delta \ln \alpha$ and $\Delta \ln c_\varepsilon$ are better for the larger α. This is because steeper density distributions contain more DM mass within the orbital radius (see Fig. 2 in [25]). In other words, the steeper density distribution has more impact on the motion of the stellar mass object and the GW waveform is modified more strongly by the DM minispike. So the DM information can be extracted from the GW waveform if the DM minihalo near the BH has a steep profile.

On the other hand, the measurement accuracy of the parameters which appear in the phase $\tilde{\Phi}(f)$ become worse in $\alpha > 2.5$. This feature can be explained by the number of GW cycles $N_{\rm cycle}$ which will be discussed in Appendix B. There we show that $N_{\rm cycle}$ falls sharply at $\alpha \sim 2.5$ (see Fig. 8). The sensitivity to the parameters which appear in the phase $\tilde{\Phi}(f)$ is amplified by the number of circles $N_{\rm cycle}$ in the frequency bandwidth of eLISA. For this reason, the measurement errors of M_c, α and c_ε increase suddenly at $\alpha \sim 2.5$, as is shown in Fig. 5. We also note that this figure shows that we can measure the power-law index α at 10% level even for a moderately flat radial distribution with $\alpha \sim 1.7$. In fact, when considering the gravitational pull due to the DM potential only, it affects detectability of GW signals only for $\alpha \gtrsim 2$. It is the dynamical friction that enables us to explore a flatter DM distribution than "a DM minispike" referred to in the literature that has $\alpha \geq 2.25$.

Figure 6 shows the relative errors of the DM parameters, α and c_ε for various values of $\rho_{\rm sp} r_{\rm sp}^\alpha$ as a function of α. As can be seen in Fig. 6, the relative errors for the fixed α become smaller approximately linearly as the DM density increases. This behavior can be traced to the amount of the DM within the orbital radius of the stellar mass object. It should be noted that the values of $\rho_{\rm sp}$ and $r_{\rm sp}$ we adopt in this paper are derived under the assumption that the initial DM minihalo profile is the NFW profile as discussed in the Sec. II. Even if the DM density is an order of magnitude more sparse than that indicated by the NFW profile, the power-law index α is measurable with an accuracy of $\Delta\alpha/\alpha < 10\%$ for $\alpha > 1.9$.

V. CONCLUSION

In this paper, we have investigated measurement accuracy of DM parameters by GW observations. We consider a binary system composed of an IMBH surrounded by a DM minispike and a stellar mass compact object. The compact object falling into the central IMBH is affected by by the gravitational interaction of both the IMBH and the DM minispike, namely the gravitational potential of both the IMBH and the DM minispike, gravitational wave back-reaction and dynamical friction. Then the resulting inspiral GW is modified by the DM minispike in comparison with the case in the absence of the DM minispike. Such a GW will be detected by future space-borne detectors such as eLISA/NGO. We derived the GW waveform modified by the minispike analytically and obtained Eqs. (28a)–(28e). We found that thanks to the DM parameters contained in the GW phase, the measurement errors of the DM parameters are very small for large power-law index of the

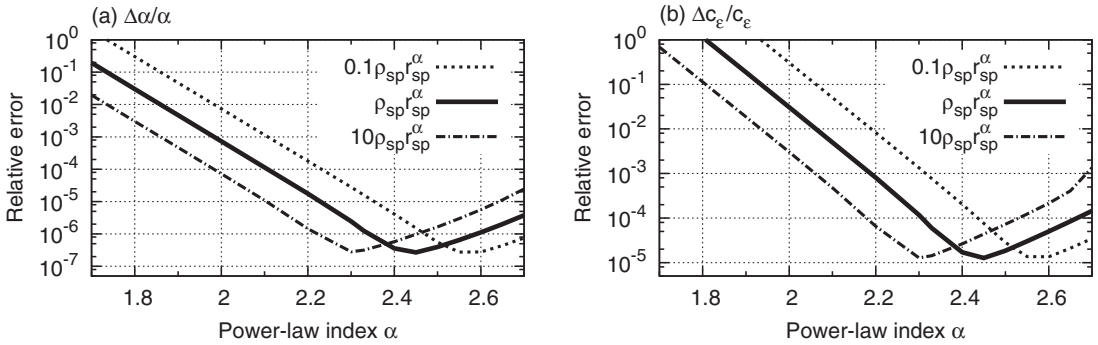

FIG. 6. The relative errors of (a) α and (b) c_ε versus the power-law index of the DM profile for $S/N = 10$ in the case where the DM minispike harboring the IMBH has a radially power-law profile. The solid line, the dashed line and the dashed-dotted line corresponds to $\rho_{\rm sp} r_{\rm sp}^\alpha$, $0.1\rho_{\rm sp} r_{\rm sp}^\alpha$, and $10\rho_{\rm sp} r_{\rm sp}^\alpha$, respectively. The values of $r_{\rm sp}$ and $\rho_{\rm sp}$ are taken from Table I.

minispike profile. To put it another way, we can extract the DM parameters very accurately from the GW waveform using matched filtering if the DM minispike has a steep profile. Indeed, in our reference case as originally advocated by [15,16], we could determine the power-law index of the DM minispike radial profile with the 1σ relative error of $\pm 5 \times 10^{-6}$ for a GW signal with signal-to-noise ratio 10 and assuming five years of observation with eLISA, as shown in Fig. 3. We also investigated how accurately the DM parameters can be determined for various values of the slope of the DM minispike and the masses of the IMBH-stellar mass object binary. We have found that smaller the mass of the stellar mass object, that of the IMBH, or the larger the power-law index of the DM minispike, we can measure DM parameters to better accuracy as shown in Figs. 4 and 5. Even a moderately flatter minispike with the radial distribution proportional to $r^{-1.7}$ would still allow us to determine the power-law index to 10% accuracy.

Indirect dark matter searches in the gamma-ray band and through GW observation proposed in our previous [25] and current papers are complementary to each other. The GW observations we propose should be applicable to both very weakly annihilating and nonannihilating DM particles. Even if the DM particles do not weakly interact with each other, in which case where we expect no gamma rays due to the DM annihilation, DM minispike affects the motion of the stellar mass object gravitationally and the resulting GW is modified by them. GW is insensitive to absorption and scattering in the interstellar medium during the propagation unlike electromagnetic waves. Therefore, GW observations offer information on the DM minispike directly. On the other hand, if the DM particles self-annihilate, an annihilation plateau may develop within a Hubble time [12] and the power-law index α of the DM radial profile becomes effectively zero within a radius $r_{\rm lim}$. For the case of the values of the parameters listed in Table I, the DM mass 200 GeV, and its cross section $\sigma v = 10^{-27}$ cm^3 s^{-1} [12], we find $r_{\rm lim} \sim 2 \times 10^{-4}$ pc which is much larger than the initial orbital radius at which the GW frequency from the binary enters the eLISA detection frequency band. In this case, the inspiral GW is unlikely to be modified by the DM minispike as indicated by Fig. 6 because the DM density within the orbital radius becomes sparse due to the DM annihilation. Hence, gamma-ray searches are a better way to explore a DM minihalo surrounding the IMBH. In summary, the GW observations probe the structure of the DM minispike, while the gamma-ray flux is given by the combination of the density, cross section, and mass of the DM particles. Therefore, the combination of gamma-ray observations with future GW observations may even offer hints that may clarify the nature of DM particles. Moreover, because the DM profile strongly depends on the formation history of the central IMBH, both types of observation may shed light on how the IMBH evolved with cosmic history.

ACKNOWLEDGMENTS

The authors thank Jun'ichi Yokoyama and Enrico Barausse for useful comments. This work is supported by the Japan Society for the Promotion of Science, the Grant-in-Aid for JSPS Fellows Grant No. 26.8636 (K. E.), the Grant-in-Aid for Young Scientists Grant No. 25800126 (Y. I.) and the MEXT Grant-in-Aid for Scientific Research on Innovative Areas, "New Developments in Astrophysics Through Multi-Messenger Observations of Gravitational Wave Sources" (Grant No. 24103005) (Y. I.).

APPENDIX A: REWRITING THE GW WAVEFORM

Our goal in this appendix is to rewrite the waveform Eq. (25a) in the form of an explicit function of GW frequency f. According to Eqs. (25a), (25b) and (25c), the GW waveform from the binary system composed of the stellar mass object and the IMBH surrounded by DM minihalo is expressed by

$$\tilde{h}(f) = \frac{1}{2} e^{i\Psi(t)} A(t) \left[\frac{2\pi}{\ddot{\Phi}(t)}\right]^{1/2}, \tag{A1a}$$

$$\Psi(t) = 2\pi f \frac{D}{c} + \tilde{\Phi}(t) - \frac{\pi}{4}, \tag{A1b}$$

$$\tilde{\Phi}(t) \equiv 2\pi f t - \Phi(t), \tag{A1c}$$

where $A(t)$ is the time-dependent amplitude defined by Eq. (24b), $\Phi(t)$ is the time-dependent phase defined by Eq. (22c), and D is the distance to the source. We proceed as follows. We start with the amplitude $A/2\sqrt{2\pi/\ddot{\Phi}}$. The frequency f can be expressed in terms of the orbital radius R which is related to the time t by Eq. (19). So the amplitude can be expressed as a function of the frequency f through the relation between t and f. Next, we tackle the phase Ψ. Finally, combining these results, we find the explicit expression of the GW waveform in the Fourier domain.

1. Rewriting the amplitude

The GW frequency $f \equiv \omega_{\rm GW}/2\pi$ which is defined by Eq. (11) is expanded in a Taylor series in a power of R:

$$\begin{aligned} f &= \frac{\omega_{\rm GW}}{2\pi} \\ &= \frac{1}{\pi}\left[\frac{GM_{\rm eff}}{R^3} + \frac{F}{R^\alpha}\right]^{1/2} \\ &= \frac{\sqrt{GM_{\rm eff}}}{\pi} R^{-3/2}\left[1 + \frac{1}{2}R^{3-\alpha}\varepsilon - \frac{1}{8}R^{2(3-\alpha)}\varepsilon^2 + \cdots\right]. \end{aligned} \tag{A2}$$

Inverting this equation, we obtain R as a function of GW frequency and expanded in ε,

$$R = \delta^{1/(3-\alpha)}\left[1 + \frac{1}{3}\delta\varepsilon + \frac{2-\alpha}{9}\delta^2\varepsilon^2 + \cdots\right], \tag{A3a}$$

$$\delta \equiv \left(\frac{GM_{\rm eff}}{\pi^2 f^2}\right)^{(3-\alpha)/3}, \tag{A3b}$$

where we introduce a new frequency variable δ defined by Eq. (A3b) for convenience. Using the definition of x given by Eq. (17), the dimensionless radius parameter x can be expanded in a power of ε,

$$x = (\delta\varepsilon)^{1/(3-\alpha)}\chi, \tag{A4a}$$

$$\chi \equiv 1 + \frac{1}{3}\delta\varepsilon + \frac{2-\alpha}{9}\delta^2\varepsilon^2 + \cdots, \tag{A4b}$$

where we introduce χ for convenience. Note that the function χ is equal to 1 when a DM minispike is not present around an IMBH.

For later convenience, we rewrite dx/dt which is defined by Eq. (19) as follows:

$$\begin{aligned}\frac{dx}{dt} &= -c_{\rm GW}\frac{(1+x^{3-\alpha})^3}{4x^3[1+(4-\alpha)x^{3-\alpha}]} \\ &\quad - c_{\rm DF}\frac{1}{(1+x^{3-\alpha})^{1/2}[1+(4-\alpha)x^{3-\alpha}]x^{-5/2+\alpha}} \\ &= -c_{\rm GW}f_{\rm GW}(x) - c_{\rm DF}f_{\rm DF}(x) \\ &= -c_{\rm GW}f_{\rm GW}(x)\left[1 + \frac{c_{\rm DF}}{c_{\rm GW}}\frac{f_{\rm DF}(x)}{f_{\rm GW}(x)}\right] \\ &= -c_{\rm GW}f_{\rm GW}(x)[1+\tilde{c}J(x)],\end{aligned} \tag{A5}$$

where functions $f_{\rm GW}(x)$, $f_{\rm DF}(x)$ and $J(x)$ and a coefficient $\tilde{c}$ are defined by

$$f_{\rm GW}(x) \equiv \frac{(1+x^{3-\alpha})^3}{4x^3[1+(4-\alpha)x^{3-\alpha}]}, \tag{A6a}$$

$$f_{\rm DF}(x) \equiv \frac{1}{(1+x^{3-\alpha})^{1/2}[1+(4-\alpha)x^{3-\alpha}]x^{-5/2+\alpha}}, \tag{A6b}$$

$$J(x) \equiv \frac{f_{\rm DF}(x)}{f_{\rm GW}(x)} = \frac{4x^{11/2-\alpha}}{(1+x^{3-\alpha})^{7/2}}, \tag{A6c}$$

$$\tilde{c} \equiv \frac{c_{\rm DF}}{c_{\rm GW}}. \tag{A6d}$$

The coefficient $\tilde{c}$ is the ratio of the dynamical friction coefficient to the gravitational radiation coefficient. So $\tilde{c}$ includes the DM information.

Next, we rewrite the second time derivative of Φ, $\ddot{\Phi}$, as a function of x. From Eq. (22c), $\ddot{\Phi}$ is expressed by

$$\begin{aligned}\ddot{\Phi}(t) &= \dot{\omega}_{\rm GW} \\ &= -(GM_{\rm eff})^{1/2}\varepsilon^{3/[2(3-\alpha)]}\frac{3+\alpha x^{3-\alpha}}{x^{5/2}(1+x^{3-\alpha})^{1/2}}\frac{dx(t)}{dt}.\end{aligned} \tag{A7}$$

To move from the first line to the second, we have made use of Eqs. (11) and (17). The time derivative of x displayed in the right-hand side of Eq. (A7) can be rewritten as a function of x by Eq. (A5). So we can express $\ddot{\Phi}$ as a function of x:

$$\begin{aligned}\ddot{\Phi}(t) &= (GM_{\rm eff})^{1/2}\varepsilon^{3/[2(3-\alpha)]}c_{\rm GW}[1+\tilde{c}J(x)] \\ &\quad \times f_{\rm GW}(x)\frac{3+\alpha x^{3-\alpha}}{x^{5/2}(1+x^{3-\alpha})^{1/2}} \\ &= (GM_{\rm eff})^{1/2}\varepsilon^{3/[2(3-\alpha)]}c_{\rm GW}[1+\tilde{c}J(x)] \\ &\quad \times \frac{3}{4}x^{-11/2}\frac{(1+x^{3-\alpha})^{5/2}(1+\alpha x^{3-\alpha}/3)}{1+(4-\alpha)x^{3-\alpha}} \\ &= (GM_{\rm eff})^{1/2}\varepsilon^{3/[2(3-\alpha)]}c_{\rm GW}[1+\tilde{c}J(x)] \times \frac{3}{4}x^{-11/2}K(x),\end{aligned} \tag{A8}$$

where the function $K(x)$ is defined by

$$K(x) \equiv \frac{(1+x^{3-\alpha})^{5/2}(1+\alpha x^{3-\alpha}/3)}{1+(4-\alpha)x^{3-\alpha}}. \tag{A9}$$

Note that $K(x)$ is equal to one when a DM minispike is not present around an IMBH.

Substitution of Eqs. (11) and (17) into Eq. (24b) gives

$$A = \frac{4G\mu}{Dc^4}(\pi f)^2\varepsilon^{-2/(3-\alpha)}x^2, \tag{A10}$$

after some algebra and simplification. Combining Eqs. (A10) and (A8), we finally arrive at the final expression for the amplitude,

$$\begin{aligned}\frac{A}{2}\sqrt{\frac{2\pi}{\ddot{\Phi}}} &= \frac{1}{2}\times\frac{4G\mu}{Dc^4}(\pi f)^2\varepsilon^{2/(3-\alpha)}x^2 \times \sqrt{\frac{8\pi}{3}}(GM_{\rm eff})^{-1/4}\varepsilon^{-3/[4(3-\alpha)]}c_{\rm GW}^{-1/2}[1+\tilde{c}J(x)]^{-1/2}x^{11/4}K(x)^{-1/2} \\ &= \sqrt{\frac{32\pi^5}{3}}\frac{G\mu}{Dc^4}(GM_{\rm eff})^{-1/4}c_{\rm GW}^{-1/2}\varepsilon^{5/[4(3-\alpha)]}f^2x^{19/4}[K(x)(1+\tilde{c}J(x))]^{-1/2} \\ &= \sqrt{\frac{5}{24}}\frac{1}{\pi^{2/3}}\frac{c}{D}\left(\frac{GM_c}{c^3}\right)^{5/6}f^{-7/6}\chi^{19/4}[K(x)(1+\tilde{c}J(x))]^{-1/2},\end{aligned} \tag{A11}$$

where M_c is defined by $M_c \equiv \mu^{3/5} M_{\rm eff}^{2/5}$ and is called the chirp mass. From the second line to the third line, we have used Eqs. (18), (20a) and (A4a).

2. Rewriting the phase

Our next task is to express the phase Ψ given by Eq. (A1b) as a function of $x = x(f)$. From Eq. (A8), the time derivative of frequency df/dt is expressed by

$$\begin{aligned}\frac{df}{dt} &= \frac{\ddot{\Phi}}{2\pi} \\ &= \frac{3}{8\pi}(GM_{\rm eff})^{1/2}\epsilon^{3/[2(3-\alpha)]}c_{\rm GW}x^{-11/2}[K(1+\tilde{c}J)] \\ &= \frac{3}{5}\pi\left(\frac{8\pi GM_c}{c^3}\right)^{5/3} f^{11/3}\chi^{-11/2}[K(1+\tilde{c}J)]. \end{aligned} \tag{A12}$$

We used Eqs. (20a) and (A4a) to go from the second line to the third line. Using Eq. (A12), we get

$$\Phi(f) = \frac{10}{3}\left(\frac{8\pi GM_c}{c^3}\right)^{-5/3}\int df' \frac{\chi^{11/2}}{f'^{8/3}K(1+\tilde{c}J)}, \tag{A13a}$$

$$2\pi f t = -\frac{10}{3}\left(\frac{8\pi GM_c}{c^3}\right)^{-5/3} f \int df' \frac{\chi^{11/2}}{f'^{11/3}K(1+\tilde{c}J)}, \tag{A13b}$$

where the constant of integration is determined by the initial condition of the GW phase.

3. Final form

Collecting the above results, Eqs. (A11), (A13a) and (A13b), we finally obtain the GW waveform in the frequency domain:

$$\tilde{h}(f) = \mathcal{A}f^{-7/6}e^{i\Psi(f)}\chi^{19/4}[K(x)(1+\tilde{c}J(x))]^{-1/2}, \tag{A14a}$$

$$\mathcal{A} = \left(\frac{5}{24}\right)^{1/2}\frac{1}{\pi^{2/3}}\frac{c}{D}\left(\frac{GM_c}{c^3}\right)^{5/6}\frac{1+\cos^2\iota}{2}, \tag{A14b}$$

$$\Psi(f) = 2\pi f\left(t_c + \frac{D}{c}\right) - \Phi_c - \frac{\pi}{4} - \tilde{\Phi}(f), \tag{A14c}$$

$$\begin{aligned}\tilde{\Phi}(f) = \frac{10}{3}\left(\frac{8\pi GM_c}{c^3}\right)^{-5/3}\Bigg[-f\int_\infty^f df' \frac{\chi^{11/2}}{f'^{11/3}K(1+\tilde{c}J)} \\ + \int_\infty^f df' \frac{\chi^{11/2}}{f'^{8/3}K(1+\tilde{c}J)}\Bigg], \end{aligned} \tag{A14d}$$

where $\mathcal{A}$ is the overall amplitude, t_c is the coalescence time and Φ_c is the coalescence phase. Note that when a DM minispike is not present around an IMBH, $\chi \to 1$, $K \to 1$, $M_c \to M_{c0} \equiv \mu^{3/5}M_{\rm BH}^{2/5}$, so the waveform becomes

$$\tilde{h}(f) = \mathcal{A}f^{-7/6}e^{i\Psi(f)}, \tag{A15a}$$

$$\mathcal{A} = \left(\frac{5}{24}\right)^{1/2}\frac{1}{\pi^{2/3}}\frac{c}{D}\left(\frac{GM_{c0}}{c^3}\right)^{5/6}, \tag{A15b}$$

$$\Psi(f) = 2\pi f\left(t_c + \frac{D}{c}\right) - \Phi_c - \frac{\pi}{4} - \tilde{\Phi}(f), \tag{A15c}$$

$$\tilde{\Phi}(f) = -\frac{3}{4}\left(\frac{GM_{c0}}{c^3}8\pi f\right)^{-5/3}. \tag{A15d}$$

This is consistent with the waveform from the binary composed of two pointlike compact objects with mass μ and $M_{\rm BH}$ [46].

APPENDIX B: THE NUMBER OF GW CYCLES

The detector sensitivity to the inspiral GWs is closely related to the number of GW cycles. That is because $N_{\rm cycle}$ which is defined by Eq. (B1) is proportional to the GW phase which is defined by Eq. (22c). Therefore, SNR strongly depends on the number of cycles $N_{\rm cycle}$. The number of GW cycles in the frequency range $f \in [f_{\rm min}, f_{\rm max}]$ is defined by

$$N_{\rm cycle} = \int_{t_{\rm min}}^{t_{\rm max}} dt f(t) = \int_{f_{\rm min}}^{f_{\rm max}} df \frac{f}{\dot{f}}, \tag{B1}$$

where an overdot denotes the time derivative and df/dt can be calculated by Eq. (39) (Note that $d\tau = -dt$.).

We define the frequency bandwidth of eLISA as the frequency range $f \in [f_-, f_+]$ within which the square root of the noise spectral density is below half its minimum value,

$$\sqrt{S_n(f)} \le 2\sqrt{S_n(f_{\rm best})}, \qquad (f \in [f_-, f_+]), \tag{B2}$$

where $f_{\rm best}$ is the frequency at which the eLISA is most sensitive to the GWs. Because we assume five years of observation, depending on the binary configuration, f_- may be smaller or larger than the initial frequency $f_{\rm ini}$ from which the inspiral GW frequency sweeps to the frequency at the innermost stable circular orbit, $f_{\rm ISCO}$. Taking the initial frequency $f_{\rm ini}$ into account, the frequency bandwidth $[f_{\rm min}, f_{\rm max}]$ in which the inspiral GW sweeps is expressed by

$$f_{\rm min} = \max\{f_{\rm ini}, f_-\}, \tag{B3a}$$

$$f_{\rm max} = \min\{f_{\rm ISCO}, f_+\}, \tag{B3b}$$

and we obtain Fig. 7 from Eq. (B1). For $\alpha < 2.5$, the initial frequency $f_{\rm ini}$ at which the GW start to be observed is within the full width at half minimum of $\sqrt{S_n(f)}$. So the minimum frequency $f_{\rm min}$ which the inspiral GW spends in

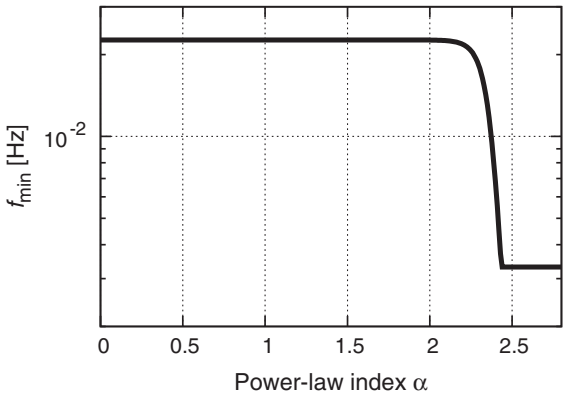

FIG. 7. Lower frequency bound which is the minimum frequency the inspiral GW spend in the detector bandwidth $[f_-, f_+]$ for $\mu = 1M_\odot$ and $M_{\rm BH} = 10^3 M_\odot$.

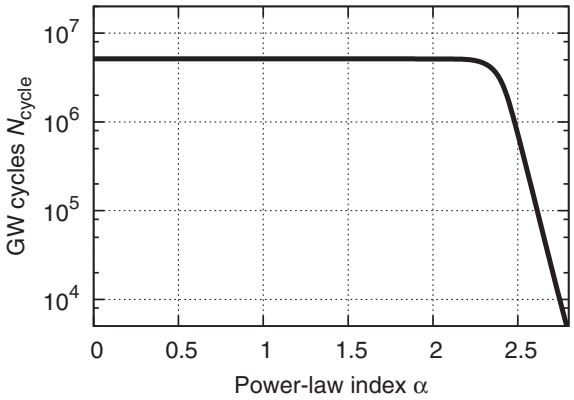

FIG. 8. The number of cycles $N_{\rm cycle}$ spent in the bandwidth $f \in [f_{\rm min}, f_{\rm max}]$ for $\mu = 1M_\odot$ and $M_{\rm BH} = 10^3 M_\odot$. For large α, the number of cycles drops sharply because of the DM effect.

the detector bandwidth is equal to the initial frequency $f_{\rm ini}$. On the other hand, for $\alpha > 2.5$, the initial frequency $f_{\rm ini}$ is out of the full width at half minimum. So $f_{\rm min}$ is equal to the lower bound of the detector bandwidth of eLISA f_-. Since f_+ is smaller than $f_{\rm ISCO}$ for all values of α and in the cases we studied, $f_{\rm max} = f_+$

Using Eqs. (39), (B1), (B3a) and (B3b), the number of cycles $N_{\rm cycle}$ is obtained in Fig. 8. The figure shows that $N_{\rm cycle}$ is almost constant for small α but drops sharply for large α. This behavior of $N_{\rm cycle}$ is explained by the fact that the DM has more influence on the motion of the stellar mass object for larger α. For large α, df/dt increases sharply as $t \to t_c$ due to the DM effect and the GW frequency of the stellar mass object goes up rapidly through the frequency bandwidth of eLISA. It follows from this that larger α leads to wider frequency band but to the less number of GW cycles near the best sensitivity of the detector. The sensitivity to the GWs is determined by the competition between these two effects.

[1] S. Arrenberg, H. Baer, V. Barger, L. Baudis, D. Bauer, J. Buckley, M. Cahill-Rowley, R. Cotta, A. Drlica-Wagner, J. L. Feng *et al.*, arXiv:1310.8621.
[2] M. Ackermann, M. Ajello, A. Albert, A. Allafort, L. Baldini, G. Barbiellini, D. Bastieri, K. Bechtol, R. Bellazzini, E. Bissaldi *et al.*, Phys. Rev. D **88**, 082002 (2013).
[3] J. Albert *et al.* (MAGIC Collaboration), Astrophys. J. **679**, 428 (2008).
[4] A. Abramowski, F. Acero, F. Aharonian, A. G. Akhperjanian, G. Anton, S. Balenderan, A. Balzer, A. Barnacka, Y. Becherini, J. Becker Tjus *et al.*, Phys. Rev. Lett. **110**, 041301 (2013).
[5] J. Grube and VERITAS Collaboration, AIP Conf. Proc. **1505**, 689 (2012).
[6] S. Funk, arXiv:1310.2695.
[7] P. Gondolo and J. Silk, Phys. Rev. Lett. **83**, 1719 (1999).
[8] T. Nakano and J. Makino, Astrophys. J. **525**, L77 (1999).
[9] P. Ullio, H. S. Zhao, and M. Kamionkowski, Phys. Rev. D **64**, 043504 (2001).
[10] D. Merritt, M. Milosavljevic, L. Verde, and R. Jimenez, Phys. Rev. Lett. **88**, 191301 (2002).
[11] D. Merritt, Phys. Rev. Lett. **92**, 201304 (2004).
[12] G. Bertone and D. Merritt, Phys. Rev. D **72**, 103502 (2005).
[13] X. Liu, Y. Shen, F. Bian, A. Loeb, and S. Tremaine, Astrophys. J. **789**, 140 (2014).
[14] E. Vasiliev, F. Antonini, and D. Merritt, Astrophys. J. **785**, 163 (2014).
[15] H.-S. Zhao and J. Silk, Phys. Rev. Lett. **95**, 011301 (2005).
[16] G. Bertone, A. R. Zentner, and J. Silk, Phys. Rev. D **72**, 103517 (2005).
[17] S. Farrell, N. Webb, D. Barret, O. Godet, and J. Rodrigues, Nature (London) **460**, 73 (2009).
[18] N. Webb, D. Cseh, E. Lenc, O. Godet, D. Barret, S. Corbel, S. Farrell, R. Fender, N. Gehrels, and I. Heywood, Science **337**, 554 (2012).
[19] D. R. Pasham, T. E. Strohmayer, and R. F. Mushotzky, Nature (London) **513**, 74 (2014).
[20] R. R. Islam, J. E. Taylor, and J. Silk, Mon. Not. R. Astron. Soc. **340**, 647 (2003).
[21] V. Rashkov and P. Madau, Astrophys. J. **780**, 187 (2014).
[22] P. Amaro-Seoane, J. R. Gair, M. Freitag, M. C. Miller, I. Mandel, C. J. Cutler, and S. Babak, Classical Quantum Gravity **24**, R113 (2007).
[23] P. Amaro-Seoane, S. Aoudia, S. Babak, P. Binetruy, E. Berti *et al.*, GW Notes **6**, 4 (2013).
[24] S. Kawamura, M. Ando, N. Seto, S. Sato, T. Nakamura *et al.*, Classical Quantum Gravity **28**, 094011 (2011).

[25] K. Eda, Y. Itoh, S. Kuroyanagi, and J. Silk, Phys. Rev. Lett. **110**, 221101 (2013).
[26] C. F. Macedo, P. Pani, V. Cardoso, and L. C. Crispino, Astrophys. J. **774**, 48 (2013).
[27] E. Barausse, V. Cardoso, and P. Pani, arXiv:1404.7140.
[28] E. Barausse, V. Cardoso, and P. Pani, Phys. Rev. D **89**, 104059 (2014).
[29] J. F. Navarro, C. S. Frenk, and S. D. M. White, Astrophys. J. **490**, 493 (1997).
[30] T. Fukushige, A. Kawai, and J. Makino, Astrophys. J. **606**, 625 (2004).
[31] A. W. Graham, D. Merritt, B. Moore, J. Diemand, and B. Terzic, Astron. J. **132**, 2685 (2006).
[32] N. Okabe and K. Umetsu, Publ. Astron. Soc. Jpn. **60**, 345 (2008).
[33] M. Oguri, A. Taruya, and Y. Suto, Astrophys. J. **559**, 572 (2001).
[34] A. R. Duffy, J. Schaye, S. T. Kay, and C. D. Vecchia, Mon. Not. R. Astron. Soc. **390**, L64 (2008).
[35] G. D. Quinlan, L. Hernquist, and S. Sigurdsson, Astrophys. J. **440**, 554 (1995).
[36] In [25], we have used $\rho_{\rm NFW}$ instead of $\rho_{\rm DM}$ to estimate $\rho_{\rm sp}$ and $r_{\rm sp}$.
[37] P. Young, Astrophys. J. **242**, 1232 (1980).
[38] G. D. Quinlan, L. Hernquist, and S. Sigurdsson, Astrophys. J. **440**, 554 (1995).
[39] L. Sadeghian, F. Ferrer, and C. M. Will, Phys. Rev. D **88**, 063522 (2013).
[40] R. Haas, R. V. Shcherbakov, T. Bode, and P. Laguna, Astrophys. J. **749**, 117 (2012).
[41] R. V. Shcherbakov, A. Pe'er, C. S. Reynolds, R. Haas, T. Bode, and P. Laguna, Astrophys. J. **769**, 85 (2013).
[42] M. MacLeod, J. Goldstein, E. Ramirez-Ruiz, J. Guillochon, and J. Samsing, Astrophys. J. **794**, 9 (2014).
[43] S. Chandrasekhar, Astrophys. J. **97**, 255 (1943).
[44] J. Binney and S. Tremaine, *Galactic Dynamics: Second Edition* (Princeton University, Princeton, NJ, 2008).
[45] M. Maggiore, *Gravitational Waves: Volume 1: Theory and Experiments* (Oxford University Press, New York, 2007).
[46] C. Cutler and E. E. Flanagan, Phys. Rev. D **49**, 2658 (1994).
[47] L. S. Finn, Phys. Rev. D **46**, 5236 (1992).
[48] P. Amaro-Seoane, S. Aoudia, S. Babak, P. Binetruy, E. Berti *et al.*, Classical Quantum Gravity **29**, 124016 (2012).
[49] C. Cutler, Phys. Rev. D **57**, 7089 (1998).